Bulletin of the Seismological Society of America, Vol. 97, No. 1A, pp. S6–S17, January 2007, doi: 10.1785/0120050624

# Comparative Analysis of the Free Oscillations Generated by the Sumatra–Andaman Islands 2004 and the Chile 1960 Earthquakes

by Carla Braitenberg and Maria Zadro

Abstract The Chile 1960 and Sumatra–Andaman Islands 2004 earthquakes are among the three greatest events that have occurred since the instrumental recording of seismic waves. The two events have similarities in hypocentral depth and focal mechanism but are very different when considering the extension of the fault plane. The recent event has close to 50% greater length than the Chile event, and although the moment magnitude of the Chile event is 0.2 to 0.5 points greater, the magnitude determination of the Sumatra–Andaman depends on the frequency range considered in the calculations (free oscillations with periods $> 1000$ sec or seismic waves, with periods of 300–500 sec). For the Chile event only the seismic moment for periods of $T < 1000$ sec is presently available, although the estimate of seismic moment at larger periods is crucial for a comparison of the two events. Our study makes a direct comparison of the free oscillation amplitudes of the two events by analyzing the records of the Grotta Gigante long-base tiltmeters, which have been recording tilt continuously since 1960. The particular mountings and physical dimension of the instruments make them particularly apt to record the torsional free oscillation waves, scarcely observed by standard long-period seismographs and not directly observable by the gravity meters. We determine the singlet frequencies for some of the lower spheroidal and torsional modes and a broad spectrum of multiplet frequencies for the higher modes. After correcting for the decay of the modes, we determine the amplitude ratios of the activated modes for the two events. The amplitude ratios vary between 1.5 and 3. Our results can be used directly for determining the ratios of the seismic moments of the two events over the frequency range 0.3–3 mHz, the only necessary correction being that of the site dependence of the free mode amplitudes.

## Introduction

The Chile 1960 and Sumatra–Andaman Islands 2004 earthquakes are among the three greatest events that have occurred since the time of seismologic recording history. They both ruptured a subducting plate with a low-angle thrust mechanism and had a hypocenter located in the upper 40 km of the earth. The Chile earthquake allowed the first observation of the free oscillation modes with long-period tiltmeters (Buchheim and Smith, 1961; Bolt and Marussi, 1962; Bozzi Zadro and Marussi, 1967; Bolt and Currie, 1975) and strainmeters (Alsop *et al.*, 1961; Benioff *et al.*, 1961). The event was preceded by foreshocks rupturing on the fault and possibly precursory ultralow-frequency (5- to 10-min period) emission of seismic waves (Kanamori and Cipar, 1974; Lund, 1983). Postseismic deformation has continued to be observed in the form of vertical movement of the coast and differential horizontal crustal movement, which has continued over a time interval of more than 35 years (Hu *et al.*, 2004). The Chile event has been determined to have a moment magnitude of $M_w$ 9.5 (Kanamori, 1977), based on observations in the period range of 300 sec of the mainshock. The seismic moment of the main event has been determined to be $2.7 \times 10^{23}$ N m (Kanamori and Cipar, 1974) and rises to $6 \times 10^{23}$ N m when including the low-frequency precursor. A similar value of $5.5 \times 10^{23}$ N m was obtained in a reevaluation by Cifuentes and Silver (1989), considering the total effect of an event divided into three subevents, for a duration of 1500 sec. The three events included a foreshock, beginning 1150 sec before the mainshock with moment $1.9 \times 10^{23}$ N m; the mainshock, with a moment of $3.2 \times 10^{23}$ N m; and an event 350 sec later, with moment of $0.4 \times 10^{23}$ N m. The uncertainty on the moment estimated is 50% (Cifuentes and Silver, 1989). The moment estimate by Cifuentes and Silver (1989) is made on vertical-component long-period seismograms using the frequency interval 1–5 mHz. The numerical modeling of the dislocation of the fault based on the presumably coseismic deformation obtains a smaller seismic moment ($M_0$ $9.4 \times 10^{22}$ N m), indicating that the seismic moment from seismic

waves may be overestimated (Barrientos and Ward, 1990). Due to the lack of a sufficient number of long-period recordings at the time of the event, the seismic moment had not been determined for lower frequencies.

The Sumatra–Andaman Islands event of 2004 showed that the correct estimate of the moment magnitude requires taking the long-period seismic waves into account (periods $> 500$ sec). In fact, the moment magnitude determined by modeling the spectral amplitudes of the free oscillation modes by a point source (Stein and Okal, 2005) returned a value of $M_w$ 9.3, considerably greater than the value ($M_w$ 9.0) obtained for the point source with equal focal mechanism that fits the seismologic records with periods of 300–500 sec (Lay *et al.*, 2005). Lay *et al.* (2005) showed that for an assumption of uniform faulting geometry, the strength of the seismic-wave excitation for periods greater than 500 sec was enhanced by a factor 1.5 to 2.5 compared with that at 300 sec, according to the fault model used. The modeling showed further that the earthquake size is underestimated when the estimate of seismic moment is made at periods too short to fully present the earthquake process.

The underestimation of seismic moment at short periods ($<$500 sec) is related to the rupture mechanism of the fault and to the physical mechanism governing it. If this is a general fact, then it should also hold for the Chile event, implying that the moment magnitude could be even greater than $M_w$ 9.5, as this value was obtained from considering seismic waves at 300-sec period.

Our study allows a direct comparison of the free-mode amplitudes of the two events. We analyze the records of one identical instrument that has remained in place since the 1960 Chile earthquake. In the 1960s and 1970s the records of the long-base tiltmeters of Grotta Gigante (Trieste Karst, Italy) had been the object of several studies on the free oscillations and contributed to the first observations to prove the existence of the theoretically predicted free modes (Bolt and Marussi, 1962; Bozzi Zadro and Marussi, 1967). We have digitized the original recordings and fulfilled the spectral analysis applying modern criteria and making it parallel to the analysis of the digital recording of the Sumatra–Andaman event. We identify the free-mode frequencies starting from a theoretical Earth model and determine the free-mode amplitudes. We normalize the amplitudes of several normal modes and overtones in order to allow for the different onset times of the records with respect to the origin time of the events, taking the $Q$-values into account. At last we determine the amplitude ratios of the two events in the frequency interval of the free modes, which will allow the inversion of the ratios of the seismic moments. Our work offers a direct link between the Chile and Sumatra–Andaman events and allows investigation as to whether the problems encountered in the estimate of seismic moment by seismic waves with periods less than 500 sec for the Sumatra–Andaman event of 2004 apply also to the Chile event.

## Fault Properties of the Chile 1960 and Sumatra–Andaman Islands 2004 Earthquakes

The Chile earthquake sequence of 1960 ruptured close to 1000 km of the southernmost section of the Nazca plate, which is being subducted beneath the South American plate along the Peru–Chile trench at a rate between 66 and 84 mm/yr to the east, the exact value depending on the work of different authors (Cifuentes, 1989; De Mets *et al.*, 1994; Angermann *et al.*, 1999). The mainshock consisted of two events, which occurred on 22 May 1960 at 19:10.40 GMT (latitude 38.06° S, longitude 72.19° W) and 19:11:14 GMT (38.17° S, 72.57° W), had a moment magnitude of $M_w$ 9.5 (Kanamori, 1977), and ruptured southward to the intersection of the Chile Ridge with the Peru–Chile trench (Cifuentes, 1989). The rupture length, estimated from the distribution of aftershocks during the first month, is $920 \pm 100$ km. According to Cifuentes (1989), the depths of the aftershocks are poorly determined, the depths for one foreshock and two aftershocks being 22 km. Talley and Cloud (1962) estimated the depth extent of aftershocks to be from the surface to a depth of 60 km. The width is not well constrained and has been estimated to be 140–190 km. The main event was preceded by a foreshock sequence that began 33 hr before the mainshock, starting with a strong event of moment $2 \times 10^{21}$ N m ($M_w$ 8.1). Barrientos and Ward (1990) developed an inversion model to infer the coseismic fault-slip distribution from surface deformation data. In their spatially variable fault-slip model, the slip varies from 0 to 40 m. If the slip was allowed to be uniform along a rectangular fault 850 km long, 130 km wide, and dipping 20°, they obtain an average slip of 17 m. The seismic moment of $9.4 \times 10^{22}$ N m ($\lambda = \mu = 5 \times 10^{10}$ Pa), which they obtain from modeling the presumably coseismic slip, is less than one fifth the total seismic moment of the 1960 sequence estimated by Kanamori and Cipar (1974) and Cifuentes and Silver (1989).

The Sumatra–Andaman earthquake of 26 December 2004 ruptured the boundary between the Indo-Australian plate and the southeastern portion of the Eurasian plate, which is segmented into the Burma and Sunda subplates. The Indo-Australian plate subducts the Eurasian plate along the Andaman trench with an oblique motion, with a convergence rate of about 14 mm/yr (Lay *et al.*, 2005). The mainshock rupture began at 3.3° N, 96.0° E, at a depth of about 30 km, at 00:58:53 GMT. The Harvard centroid moment tensor (CMT) solution indicates predominantly thrust faulting on a shallowly (8°) dipping plane with a strike of 329°. The rake (110°) indicates a slip direction about 20° closer to the trench-normal direction than to the interplate convergence direction (Lay *et al.*, 2005). The extent of the fault plane estimated from the aftershock distribution is of 1300-km length, with 240-km width in the southern portion of the thrust, extending to a depth of about 45 km (northwestern Sumatra). In the northern portion, the plane is 160 to 170 km wide, extending to a depth of 30 km (Lay *et al.*, 2005). The Harvard CMT solution of the mainshock, based on record-

ings of 300- to 500-sec-period surface waves, has a seismic moment $M_0 = 4.0 \times 10^{22}$ N m and a moment magnitude $M_w$ 9.0. The estimate of the moment magnitude of the Chile earthquake was made from measurements at comparable periods of the surface waves (300 sec) (Kanamori, 1977; Kanamori and Cipar, 1974) and is thus directly comparable to this value. Extending the analysis of the 2004 event to longer periods has shown that the seismic moment is underestimated when considering periods limited to 500 sec. By considering the gravest free oscillation modes with $T >$ 1000 sec, it resulted that the amplitudes of the spheroidal free oscillations were a factor 1.25 to 2.6 larger than those predicted by the Harvard CMT source (Stein and Okal, 2005). In order to explain the observed amplitudes, the same authors estimate the earthquake magnitude to be $M_w$ 9.3, assuming a shallow-dipping (8°) thrust fault, with the same mechanism as the CMT solution and a point-source model. The finite-source models (Ammon *et al.*, 2005) obtained on long-period seismograms in the period range 100 to 3000 sec and regional and teleseismic surface waves in the period range 50 to 500 sec produced a total seismic moment of $6.5 \times 10^{22}$ N m, which is one and a half the seismic moment predicted by the CMT moment estimate at 300 sec. The finite-fault models explain the long-period free-mode amplitudes within 10%.

## The Data Series of the Chile 1960 and Sumatra 2004 Earthquakes

The Grotta Gigante (Giant Cave) situated in the Trieste Karst (latitude 45.7083° N, longitude 13.7633° E) bears the Guinness Award for the greatest cave in the world; it has an ellipsoidal shape of 130-m length, 65-m width, and 107-m height. In 1959 Antonio Marussi had the idea to use the height of the cave to build a couple of long-base tiltmeters of the horizontal pendulum type with Zöllner suspension (Marussi, 1959). The mechanical parts of the first instruments were overhauled and the present instrumentation was installed in 1966. The horizontal pendulums consist of a subhorizontal pendulum arm suspended by an upper wire fixed at the vault of the cave and a lower wire fixed to the ground of the cave. The distance between upper and lower mountings is 95 m. The total weight of the pendulum (including wires) is 18.7 kg, the horizontal beam has a length of 1.4 m, and the period of oscillation of the pendulum in the horizontal plane is presently kept at 6 min (Marussi, 1959; Braitenberg, 1999; Braitenberg and Zadro, 1999; Zadro and Braitenberg, 1999). A horizontal shift of the upper relative to the lower mounting of the pendulum (shear), a tilt of the cave, or the inclination of the vertical are recorded as a rotation of the beam in the horizontal plane about the rotation axis, which lies on the line connecting the upper and lower mounting points of the pendulum. The static amplification factor for tilt is about 24,000. The original recording system was optical on photographic paper, with an amplification of 0.9 msec/mm. This system is very reliable and has been recording without greater problems since the time of the installation. The pendulums have been overhauled in 1982–1983 and in 1997, and some parts as the polyethylene tubes protecting the wires have been exchanged. Recently, in December 2003, a new digital acquisition system was installed (Braitenberg *et al.*, 2004, 2005). The advantages given by the digital acquisition system are the automatic readout and a drastically increased time and signal resolution, wherefore the instruments acquire the characteristics of a very broadband tiltmeter. The recordings are continuously available with hourly sampling since 1966, the older data having been manually digitized from photographic recording. The digital acquisition system has a sampling rate of 109,660 data points/hr. The pendulum masses have been exchanged since the Chile recording, but the former instrumental response function is well documented (e.g. Marussi, 1959; Bolt and Marussi, 1962) so as to allow the direct comparison of the amplitudes of both earthquakes. For the Chile earthquake the original photographic recording was digitized with a sampling of 30 sec using enlargements of the original recordings. The digitized record starts 4–5 hr (east–west, 304 min; north–south, 229 min) after the origin time of the event, as the first hours were hardly readable in the photographic records. The Sumatra–Andaman event was resampled at a sampling interval of 15 sec in order to reduce the total amount of data. The original data series were detrended by least-squares adjustment of a cubic function and four oscillations, with the frequencies of the principal tidal waves (M2, S2, O1, K1). For illustration purposes the data were bandpass filtered with cutoff periods of 3 min and 3 hr (cosine-taper frequency filter). The filtered data series of the Sumatra–Andaman is shown in Figure 1 for a length of 24 hr; the record of the Chile event is shown in Figure 2 for a length of 48 hr. The spectral analysis is made on the detrended, nonfiltered data. The epicentral distances between the Trieste station and the two events are 114° and 82° for the Chile and Sumatra events, respectively. The azimuths of the Trieste station with respect to the local meridian passing through the epicenter of the events are 50° (east from north) and 44° (west from north) for the Chile and Sumatra events, respectively. Taking into account that the time series of the Chile event starts 4–5 hr after the origin time of the event, comparison of the two graphs shows that the amplitude of the Chile earthquake is significantly higher than that of the Sumatra event.

## Spectral Analysis Method

The method we have applied to find the free oscillations that were excited by the Sumatra–Andaman and Chile earthquakes was chosen with the requirement of being a simple and easily reproducible method. The possible problems are contamination of data series by noise, reduction of spectral leaking by neighboring frequencies, and the exponential decay of the modes. We therefore rely on the calculation of the Fourier spectrum of the windowed data series. For the

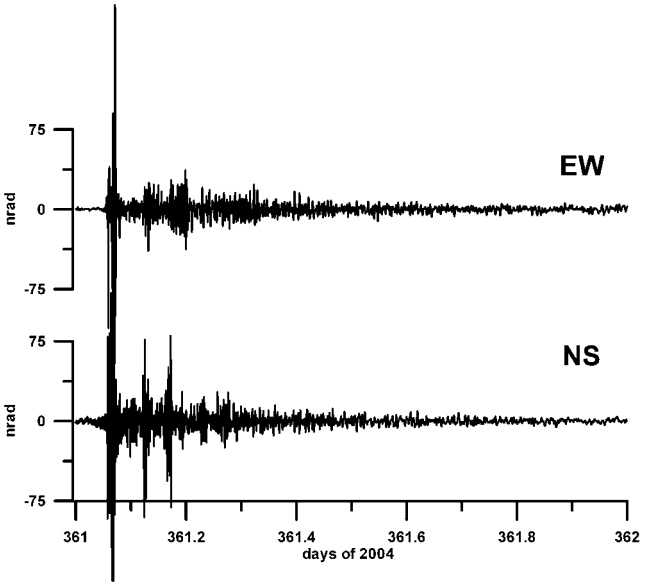


Figure 1. The record of the Sumatra–Andaman earthquake of 2004. The original recordings have been cleaned from the Earth tides, a cubic trend, and high-pass filtered. Grotta Gigante long-base pendulums. The north–south component has been clipped in the graph, as the peak values in the initial part of the signal extended from −588 to 1027 nrad.

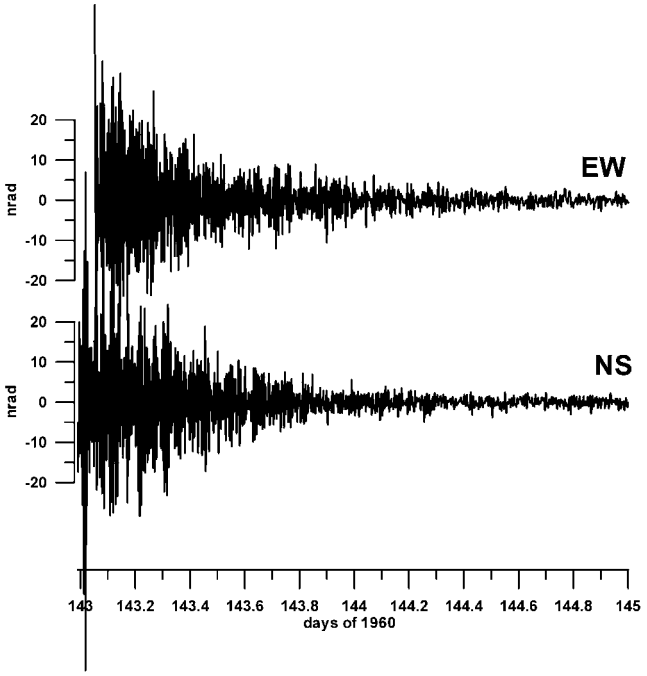


Figure 2. The record of the Chile earthquake 1960. The original recordings have been cleaned from the earth tides, a cubic trend, and high-pass filtered. Grotta Gigante long-base pendulums.

data series of $N$ equidistant samples (sampling interval $dt$), $K$ spectra were calculated for different lengths of data series, the time intervals ranging from the maximum window size of $T_{\max} = (N - 1)dt$, decreasing to $T_K = (N - 1)dt - (K - 1)dt_k$, $dt_k$ a time interval suitably chosen. The $K$ spectra thus have different resolved frequencies $f_{nK} = (n - 1)/T_K$, with $n = 1,2, \ldots ,(N - Kdt_k/dt)/2$. The different $K$ spectra are merged into a single composite spectrum. The advantage of this procedure with respect to a single spectrum is that the presence of spectral peaks that possibly fall between two resolved frequencies of the single spectrum are retrieved unambiguously. We apply a cosine-taper window function, which is flat for one-third length of the data series, and defined by

$$w(t) = \begin{cases} \sin\left(\dfrac{\pi t}{2Mdt}\right) & \text{for} \quad 0 \le t \le M\ dt \\ 1 & \text{for} \quad M\ dt \le t \le (N - M)\ dt, \\ \cos\left(\dfrac{\pi(t - (N - M)\ dt)}{2Mdt}\right) & \text{for} \quad (N - M)\ dt \le t \le N\ dt \end{cases}$$

with $M = N/3$. The choice of the width $M$ of the tapering window was made on the basis of test runs on synthetic data series mimicking the recorded signal. The cosine-taper windows were tested for different widths ($M$) of the taper function. The necessity of reducing leaking from the sidelobes requires $M = N/2$ or $M = N/3$, the higher value of $M$ implying a loss in spectral resolution. We found that the value of $M = N/3$ gave satisfactory results in the synthetic cases. The results are not significantly altered by the choice of $M = N/2$ or $M = N/3$. The application of the window function reduces the spectral amplitudes, for which reason we normalize the window function by the sum of the window weights. We illustrate the method on a test series: the synthetic data series consists of four damped oscillations (18,000 data points with 15-sec sampling) with amplitudes ($A_i$) and periods ($T_i$) with $i = 1,4$. The amplitudes and periods are $A_1 = 5.0$, $T_1 = 232$ min; $A_2 = 4.5$, $T_2 = 228$ min; $A_3 = 3.0$, $T_3 = 219$ min; and $A_4 = 1.5$, $T_4 = 202$ min with different phases. The curves are affected by Gaussian noise, with root mean square (rms) amplitude equal to 1. The decay of the amplitude of the oscillations is exponential, with a reduction of the amplitudes to 4% of the initial value over the entire time interval. The length of the data series is 18,000 samples with 15-sec sampling interval. The data series is graphed in the upper part of Figure 3. The spectral amplitudes are given in the lower part of Figure 3, where the different curves represent the standard Fourier spectrum

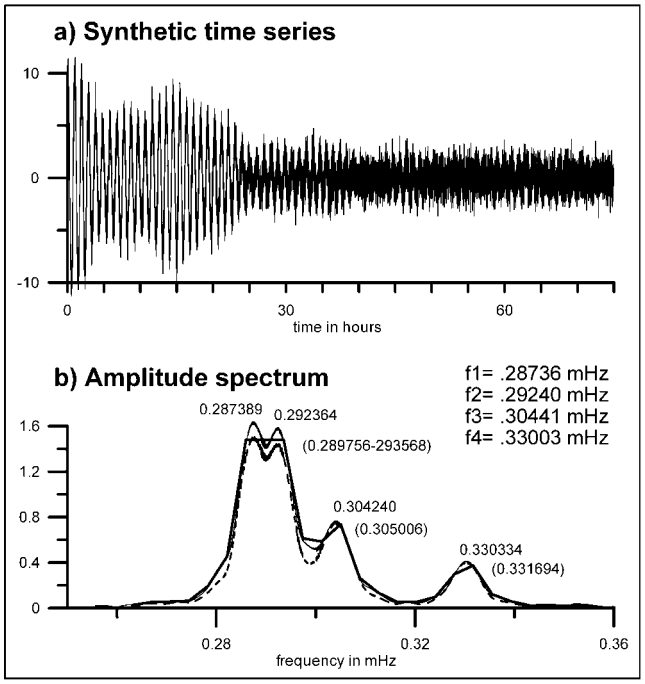


Figure 3. (a) Time series. (b) Amplitude spectrum of the synthetic data series (four damped oscillations). The different curves have been obtained with a simple Fourier spectrum with windowing (heavy line), with the composite Fourier spectrum (see text) using a tapering window with taper-width $M = N/2$ (dashed) and $M = N/3$ (light continuous line).

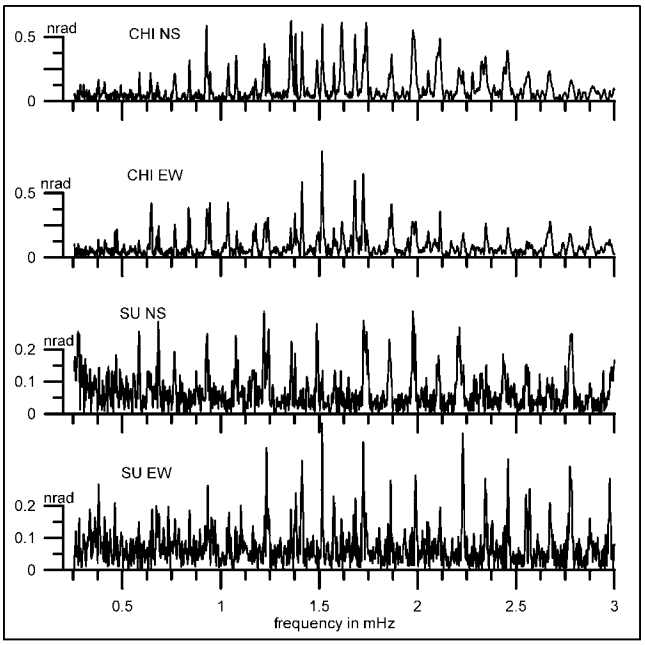


Figure 4. Amplitude spectrum for the Sumatra–Andaman and Chile earthquakes, north–south and east–west components, respectively.

with a tapered window ($M = N/3$) (segmented line), and the composite spectrum with two types of taperings ($M = N/3$, continuous line, and $M = N/2$, broken line). It can be seen that the spectral amplitudes are better resolved with the composite spectrum, particularly at lower frequencies, whereas the choice of the $M = N/3$ window allows a better determination of the amplitudes. The standard Fourier spectrum would result in a frequency shift of the identified spectral values, whereas the composite spectrum gives the correct value. The resolved spectral amplitudes are lower than the amplitude values of the synthetic oscillations due to the damping.

## Spectral Analysis Results

The spectral analysis of the recordings of the two events has been carried out using identical record lengths and procedures. The combined spectra are calculated considering three spectral windows limited by the frequency intervals 0.2–1.4 mHz, 1.2–2.4 mHz, 2.3–3.2 mHz, respectively. For each spectral window, the analysis is made on $2L + 1$ data series of $N = 17740 \pm K_i$ samples, with $i = -L, \ldots, 0, \ldots, L$ and $K_i = dK \times i$. Regarding the Sumatra–Andaman event, for the lowest spectral windows the value of $dK$ is 8, 4, and 4, with a maximum value $K_L$ of 254, 50, and 12 for the three spectral windows with increasing middle frequency, respectively. For the Chile event, which has the double sampling interval, the previous $K_i$ values have been divided by two. The complete spectra are graphed in Figure 4, and the presence of the spectral peaks indicating the activation of an entire spectrum of free oscillation is evident. The spectral amplitudes of the Sumatra–Andaman event are generally smaller compared to the Chile earthquake and distributed over a broader range of frequencies (0.5–3 mHz). The spectral amplitudes of the Chile event are concentrated on the interval between 1 and 2 mHz.

We proceed with the analysis of the spectrum by searching for spectral peaks coinciding with the singlet mode frequencies predicted by Dahlen and Sailor (1979) using the Earth model 1066A for a rotating and elliptical Earth. For frequencies greater then 0.7 mHz, we adopt the multiplet frequency corrected for ellipticity, as the singlets cannot be resolved. For frequencies greater than 2 mHz the frequencies were furnished by Walter Zürn, Schildach Observatory (personal comm, 2005) and refer to the Earth model 1066A. The list of identified modes is reported in Table 1, where the frequencies of the spectral peaks observed in each of the north–south and east–west components and for both events are given (columns 2, 3, 4, 5, of Table 1). We also give the average frequency (column 6) of all observed frequencies belonging to one multiplet and the percentual root mean square (rms) deviation (column 7), as well as the percentual rms deviation (column 9) of the observed frequencies from the theoretical multiplet frequency (column 8). The last column gives the number of observations used for calculating the averages. We find that generally the rms deviation is

Table 1
Frequencies of the Observed Earth Free Modes

| Mode | Frequency CHI–EW (mHz) | Frequency CHI–NS (mHz) | Frequency SU–EW (mHz) | Frequency SU–NS (mHz) | Average Frequency | % Rms Deviation from Mean | Model Frequency | % Rms Deviation from Model Frequency | Number of Values for Average |
|---|---|---|---|---|---|---|---|---|---|
| 0S2, $m = 0$ | — | 0.3094 | — | — | 0.3091 | 2.11405 | 0.30949 | 2.11514 | 5 |
| $m = -2$ | — | — | — | 0.3006 | | | | | |
| $m = -1$ | — | 0.3035 | — | — | | | | | |
| $m = 1$ | — | 0.3133 | — | 0.3125 | | | | | |
| $m = 2$ | — | 0.3187 | — | — | | | | | |
| 0T2, $m = 0$ | 0.3789 | 0.3787 | 0.3795 | 0.3795 | 0.37902 | 1.06264 | 0.37949 | 1.06862 | 6 |
| $m = -2$ | — | 0.3718 | — | — | | | 0.37527 | | |
| $m = +2$ | — | — | 0.3857 | — | | | 0.38300 | | |
| 2S1, $m = 0$ | — | — | — | 0.4043 | 0.4067 | 1.13968 | 0.40462 | 1.2556 | 5 |
| $m = -1$ | — | — | — | 0.3987 | | | 0.39861 | | |
| $m = +1$ | 0.4112 | 0.4096 | 0.4097 | | | | 0.41079 | | |
| 0S3 $m = 0$ | — | — | — | 0.4689 | 0.4665 | 0.99995 | 0.4687 | 1.10039 | 8 |
| $m = -3$ | — | 0.4624 | 0.4623 | 0.4607 | | | | | |
| $m = -2$ | 0.4639 | — | — | — | | | | | |
| $m = -1$ | — | 0.4672 | — | — | | | | | |
| $m = 2,3$ | 0.4728 | 0.4738 | — | — | | | | | |
| 0T3, $m = 0$ | — | 0.5873 | — | — | 0.5853 | 0.21064 | 0.58752 | 0.43222 | 4 |
| $m = -2$ | 0.5845 | — | 0.5841 | 0.5853 | | | | | |
| 0S4, $m = 0$ | — | — | — | — | 0.64668 | 0.48371 | 0.64711 | 0.48786 | 6 |
| $m = -3$ | — | 0.6429 | 0.6437 | — | | | | | |
| $m = -2$ | — | — | — | 0.6448 | | | | | |
| $m = 1$ | 0.6482 | 0.6488 | — | — | | | | | |
| $m = 4$ | — | — | 0.6517 | — | | | | | |
| 1S2, $m = 0$ | — | 0.6791 | — | — | 0.67926 | 0.65697 | 0.68093 | 0.69989 | 7 |
| $m = -2$ | — | — | 0.6729 | 0.6745 | | | | | |
| $m = -1$ | 0.6765 | — | — | — | | | | | |
| $m = 1$ | — | — | 0.6845 | 0.6825 | | | | | |
| $m = 2$ | 0.6848 | — | | — | | | | | |
| 0T4 | 0.7667 | 0.7674 | 0.7674 | 0.7652 | 0.76667 | 0.11716 | 0.76747 | 0.1563 | 4 |
| 0S5 | 0.8366 | 0.8415 | 0.8422 | — | 0.84082 | 0.29689 | 0.8404 | 0.30132 | 4 |
| | 0.843 | — | — | — | | | | | |
| 0T5 | 0.9295 | 0.9278 | 0.9341 | 0.9265 | 0.93062 | 0.32376 | 0.93035 | 0.32512 | 6 |
| | 0.9346 | — | — | 0.9312 | | | | | |
| 1S3 | 0.9452 | 0.935 | — | 0.9384 | 0.94206 | 0.48883 | 0.94121 | 0.49753 | 5 |
| | — | 0.9473 | — | 0.9444 | | | | | |
| 3S1 | 0.9452 | 0.935 | — | 0.9384 | 0.94206 | 0.48883 | 0.94272 | 0.49348 | 5 |
| | — | 0.9473 | — | 0.9444 | | | | | |
| 2S2 | — | — | 0.9522 | — | 0.95455 | 0.24619 | 0.95375 | 0.26039 | 2 |
| | — | — | 0.9569 | — | | | | | |
| 0S6 | 1.0367 | 1.0391 | 1.0317 | — | 1.04016 | 0.62624 | 1.03802 | 0.66053 | 5 |
| | — | — | 1.042 | — | | | | | |
| | — | — | 1.0513 | — | | | | | |
| 0T6 | 1.0814 | 1.0786 | 1.0747 | 1.0702 | 1.07867 | 0.4701 | 1.08121 | 0.52449 | 7 |
| | — | — | 1.0821 | 1.0767 | | | | | |
| | — | — | — | 1.087 | | | | | |
| 3S2 | — | — | 1.1022 | — | 1.1022 | — | 1.10772 | 0.49832 | 1 |
| 1S4 | 1.1668 | 1.1766 | 1.1639 | 1.1616 | 1.17093 | 0.57034 | 1.17454 | 0.6464 | 7 |
| | 1.1788 | — | — | 1.1699 | | | | | |
| | — | — | — | 1.1789 | | | | | |
| 0T7 | 1.2223 | 1.2228 | 1.2238 | 1.22 | 1.22334 | 0.20883 | 1.22318 | 0.20926 | 5 |
| | 1.2278 | — | — | — | | | | | |
| 0S7 | — | 1.2325 | 1.2327 | 1.2302 | 1.2318 | 0.09208 | 1.23142 | 0.09714 | 3 |
| 2S3 | 1.2402 | 1.2457 | 1.2411 | 1.2442 | 1.2428 | 0.18001 | 1.24181 | 0.19701 | 4 |
| 0T8 | 1.3556 | 1.3574 | 1.3567 | 1.3597 | 1.35735 | 0.11057 | 1.35887 | 0.1572 | 4 |
| 2S4 | 1.3772 | 1.3797 | 1.3811 | 1.3774 | 1.3799 | 0.18521 | 1.37861 | 0.20766 | 5 |
| | 1.3841 | — | — | — | | | | | |
| 0S8 | 1.4128 | 1.4131 | 1.4129 | — | 1.41293 | 0.00883 | 1.41279 | 0.01345 | 3 |

(*continued*)

Table 1
Continued

| Mode | Frequency CHI–EW (mHz) | Frequency CHI–NS (mHz) | Frequency SU–EW (mHz) | Frequency SU–NS (mHz) | Average Frequency | % Rms Deviation from Mean | Model Frequency | % Rms Deviation from Model Frequency | Number of Values for Average |
|---|---|---|---|---|---|---|---|---|---|
| 0T9 | 1.4895 | 1.4892 | — | 1.4871 | 1.491 | 0.21712 | 1.4897 | 0.23418 | 5 |
| | 1.4963 | — | — | 1.4929 | | | | | |
| 2S5 | 1.5152 | 1.5165 | 1.5155 | 1.5175 | 1.51618 | 0.05961 | 1.51456 | 0.1222 | 4 |
| 1S6 | 1.5152 | 1.5165 | 1.5155 | 1.5175 | 1.51618 | 0.05961 | 1.52301 | 0.45269 | 4 |
| 0S9 | 1.5747 | 1.576 | 1.5737 | 1.5803 | 1.57617 | 0.15971 | 1.57689 | 0.16595 | 4 |
| 0T10 | 1.6166 | 1.6151 | 1.6132 | 1.6104 | 1.61383 | 0.14349 | 1.61725 | 0.25564 | 4 |
| 2S6 | 1.6821 | 1.6825 | 1.6738 | — | 1.6808 | 0.24814 | 1.68121 | 0.24928 | 4 |
| | — | — | 1.6848 | — | | | | | |
| 0S10 | 1.7243 | 1.7258 | 1.7241 | 1.7256 | 1.72495 | 0.04386 | 1.72326 | 0.10745 | 4 |
| 0T11 | 1.7413 | 1.7393 | 1.7375 | 1.7407 | 1.7397 | 0.08409 | 1.74286 | 0.1998 | 4 |
| 0T12 | 1.8569 | 1.8682 | 1.8625 | 1.8565 | 1.86228 | 0.26595 | 1.83044 | 1.76039 | 5 |
| | 1.8673 | — | — | — | | | | | |
| 0S11 | 1.8569 | 1.8682 | 1.8625 | 1.8565 | 1.86228 | 0.26595 | 1.89257 | 1.62172 | 5 |
| | 1.8673 | — | — | — | | | | | |
| 0T13 | 1.9741 | 1.9765 | — | 1.9763 | 1.97563 | 0.05504 | 1.97631 | 0.0648 | 3 |
| 0S12 | 1.9907 | — | 1.9901 | 1.9889 | 1.9899 | 0.03761 | 1.99393 | 0.20557 | 3 |
| 2S8 | 2.0546 | 2.0537 | — | — | 2.05415 | 0.02191 | 2.05097 | 0.1565 | 2 |
| 0S13 | 2.1144 | 2.1135 | 2.1146 | 2.1069 | 2.11235 | 0.15025 | 2.11289 | 0.15237 | 4 |
| 0T15 | — | 2.2099 | — | 2.2024 | 2.2084 | 0.19996 | 2.21405 | 0.32392 | 3 |
| | — | — | — | 2.2129 | | | | | |
| 0S14/2S9 | 2.232 | 2.2303 | 2.2288 | 2.233 | 2.23102 | 0.07202 | 2.23144 | 0.07439 | 4 |
| 0T16 | — | 2.325 | — | — | 2.325 | — | 2.32896 | 0.16991 | 1 |
| 0S15 | 2.3465 | 2.3449 | 2.3441 | 2.349 | 2.34612 | 0.07976 | 2.34655 | 0.08179 | 4 |
| 6S2 | — | 2.4396 | — | 2.4349 | 2.43863 | 0.11237 | 2.43764 | 0.11963 | 3 |
| | — | — | — | 2.4414 | | | | | |
| 0T17 | — | 2.4396 | — | 2.4349 | 2.43863 | 0.11237 | 2.44291 | 0.20792 | 3 |
| | — | — | — | 2.4414 | | | | | |
| 0S16 | 2.4594 | 2.4567 | 2.4597 | 2.4576 | 2.45835 | 0.05068 | 2.45854 | 0.05125 | 4 |
| 0T18/3S6 | 2.5557 | — | 2.5505 | 2.5531 | 2.5531 | 0.08315 | 2.55608 | 0.14308 | 3 |
| 0S17 | 2.5664 | 2.5627 | 2.5693 | 2.5615 | 2.56538 | 0.11199 | 2.56761 | 0.14164 | 5 |
| | — | — | — | 2.567 | | | | | |
| 0S18 | 2.673 | 2.6718 | 2.6727 | — | 2.6725 | 0.01908 | 2.67396 | 0.05798 | 3 |
| 2S12 | 2.7395 | — | — | — | 2.7395 | — | 2.74017 | 0.02452 | 1 |
| 0S19 | 2.7728 | 2.7743 | 2.7762 | 2.7825 | 2.77717 | 0.11824 | 2.7778 | 0.12038 | 6 |
| | 2.7772 | 2.78 | — | — | | | | | |
| 0T20 | 2.7728 | 2.7743 | 2.7762 | 2.7825 | 2.77717 | 0.11824 | 2.78059 | 0.17049 | 6 |
| | 2.7772 | 2.78 | — | — | | | | | |
| | 2.8763 | — | 2.8753 | 2.8753 | 2.87563 | 0.0164 | 2.87933 | 0.1295 | 3 |
| 0S21 | 2.9759 | — | 2.9764 | — | 2.97615 | 0.0084 | 2.97879 | 0.08912 | 2 |
| 0T22 | — | — | — | 2.9855 | 2.9974 | 0.34925 | 3.00333 | 0.40054 | 4 |
| | — | — | — | 2.9906 | | | | | |
| | — | — | — | 3.0006 | | | | | |
| | — | — | — | 3.0129 | | | | | |
| 0S22 | 3.0601 | — | — | — | 3.0601 | — | 3.07642 | 0.53032 | 1 |

smaller among the observed frequencies with respect to the theoretical model frequency, implying that the model frequency could be improved for some of the modes. For the lower-degree modes, the table row with the name of the mode gives the frequencies for azimuthal order number $m = 0$; the next lines give the resolved frequencies for $m \neq 0$. Only those order numbers are included in the table for which at least one observation was generated; the others are omitted.

Where available, the identified singlets have been reported; for the higher modes only the frequency of the multiplet is given, as the spectral vicinity of the singlets does not allow their resolution. (See Data Source section.)

The mode of lowest degree we observe is ${}_0S_2$ in the spectrum of the Chile earthquake, although some doubts are present because the amplitude is low compared to the noise level and because the influence of seiches in the Trieste gulf, with close to 1-hr period, cannot be excluded. The higher modes, starting from ${}_0T_2$, are mostly observed on both spectra, with different activation of the singlets. The data series differ in the onset of the interval after the origin time of the event. This is because the recordings of the Chile event are

only available starting some hours after the origin time (east–west, 304 min; north–south, 229 min), whereas the records of the Sumatra–Andaman event have a complete record of the event. In order to limit the disturbing effect of the high-amplitude earthquake trace, the first 46 min have been discarded in the spectral analysis of the Sumatra–Andaman event. The different delays of the time series with respect to the origin time affects the computed spectral amplitudes due to the damping of the free oscillation modes. The damping is known theoretically through the quality factor $Q$ for each oscillation mode. In order to have directly comparable amplitudes for the two events, we correct the spectral amplitudes of the identified poloidal, toroidal fundamental modes and overtones for the greater delay of the Chile event with respect to the Sumatra–Andaman event. The correction is made by multiplying the amplitudes of each mode by $\exp(\pi fT/Q)$, where $f$ is the mode frequency, and $T = t_{\mathrm{Chi}} - t_{\mathrm{Su}}$, where $t_{\mathrm{Chi}}$, $t_{\mathrm{Su}}$ are the time delays of the time series with respect to the origin times of the two events, respectively. The $Q$-values refer to the same model as the normal mode frequencies. Alternatively we could use compilations of observed $Q$, as the ones published by the Harvard University and Colorado University (e.g., website of group The reference model, http://mahi.ucsd.edu/Gabi/rem.html). We prefer using the theoretical $Q$ for the reason that the compilations show some discrepancies among different authors. In any case the use of the theoretical or experimental $Q$-values makes no significant difference in the amplitude corrections, the differences in amplitude amounting the most to 1%.

The amplitudes of the identified peaks are shown in Figure 5. The identified poloidal and toroidal fundamental modes observed on the north–south component are graphed in Figure 5a, whereas those observed on the east–west component are graphed in Figure 5b. The amplitudes for the overtones with overtone index $n = 2$ are shown in Figure 5c. We have preferred to limit the overtones to the series of index $n = 2$ and not include the other few overtones observed in the frequency interval between 0 and 3 mHz. This is because the overtones of a particular degree share the same radial function and therefore respond to common properties of the internal earth distribution. The overtones of index $n = 2$ constitute a complete series of identified excited modes, whereas the overtones of smaller or greater degree are only present with a few isolated representatives (see Table 1).

In order to quantitatively compare the two earthquakes in terms of the free-oscillation spectra, we build the amplitude ratios at those frequencies that were observed for both events. First the amplitudes of the observed modes are calculated for each event and free mode from the root of the summed squares of the north–south and east–west components. Then, the amplitude for the Chile event is divided by the amplitude of the Sumatra–Andaman event. The amplitude ratios (Fig. 6) of the free modes show that generally the Chile event has greater amplitudes with respect to the Sumatra–Andaman event by a factor ranging between 1.5 and 3. For both poloidal and toroidal modes, the lowest order modes have relatively small amplitude ratios. The mode ${}_0T_{10}$ has an anomalously high ratio (5), not found for any other mode. Only a specific modeling of the free-mode amplitudes can verify whether the presence of a nodal plane is responsible for this high value.

## Conclusion

The occurrence of the Sumatra–Andaman 2004 event has renewed the interest in the Chile 1960 event, which was the greatest event in the instrumental seismologic history. The quantification of the magnitude of the Chile event and its comparison to the Sumatra–Andaman event is presently an unresolved problem, due to the lack of well-calibrated long-period records of the Chile event.

For great earthquakes the moment magnitude is used to quantify an earthquake. It is derived from the seismic moment, which is equal to the fault area multiplied by the average static offset and by the rigidity. The seismic moment is therefore defined at zero frequency. To estimate it, seismographic recordings of long-period seismic waves are used. The magnitude of the 1960 Chile and 1964 Alaska earthquakes and the Harvard CMT–based moment magnitude of the Sumatra–Andaman 2004 event were all estimated from measurements around 300 sec. Another means to determine the seismic moment is to model the observed free oscillation modal amplitudes for the lowest modes (e.g., ${}_0S_2$, ${}_0S_3$, ${}_0S_4$, or ${}_0T_2$, ${}_0T_3$, ${}_0T_4$). For the Sumatra–Andaman earthquake it resulted that the point-source model used for modeling the observed seismic waves and model amplitudes required a seismic moment that was larger at the lowest free modes compared to the one required to explain the 300-sec seismic waves (Lay *et al.*, 2005; Park *et al.*, 2005; Stein and Okal, 2005). The $M_{\mathrm{w}}$ 9.3 moment magnitude value (Park *et al.*, 2005) refers to modeling the amplitudes of the free oscillations by a point source; a lower magnitude ($M_{\mathrm{w}}$ 9.1) is obtained from modeling long-period seismic waves with a finite-source model (periods between 100 and 3000 sec and teleseismic surface waves with period range of 50 to 500 sec). The moment magnitude obtained from long-period seismic waves with period less than 500 sec and a point source is the lowest ($M_{\mathrm{w}}$ 9.0). This raises the question whether the Chile magnitude of $M_{\mathrm{w}}$ 9.5 is underestimated as well, or whether the Sumatra–Andaman event had a particular low-frequency emission accompanied by a relatively big fault area. Our study allows the direct quantitative and comparative analysis of the two events in the frequency range of the free oscillations. The long-base tiltmeters of the Grotta Gigante are ideal for the detection of the free oscillation modes, due to their long-period eigenfrequency (6–9 min). The presently existing instrument is the same as the one that recorded the Chile 1960 event, leaving no doubts on the calibration factor and exact positioning of the instrument. In the present stage of our study, we have made a detailed, spectral analysis of the two events and have extracted the

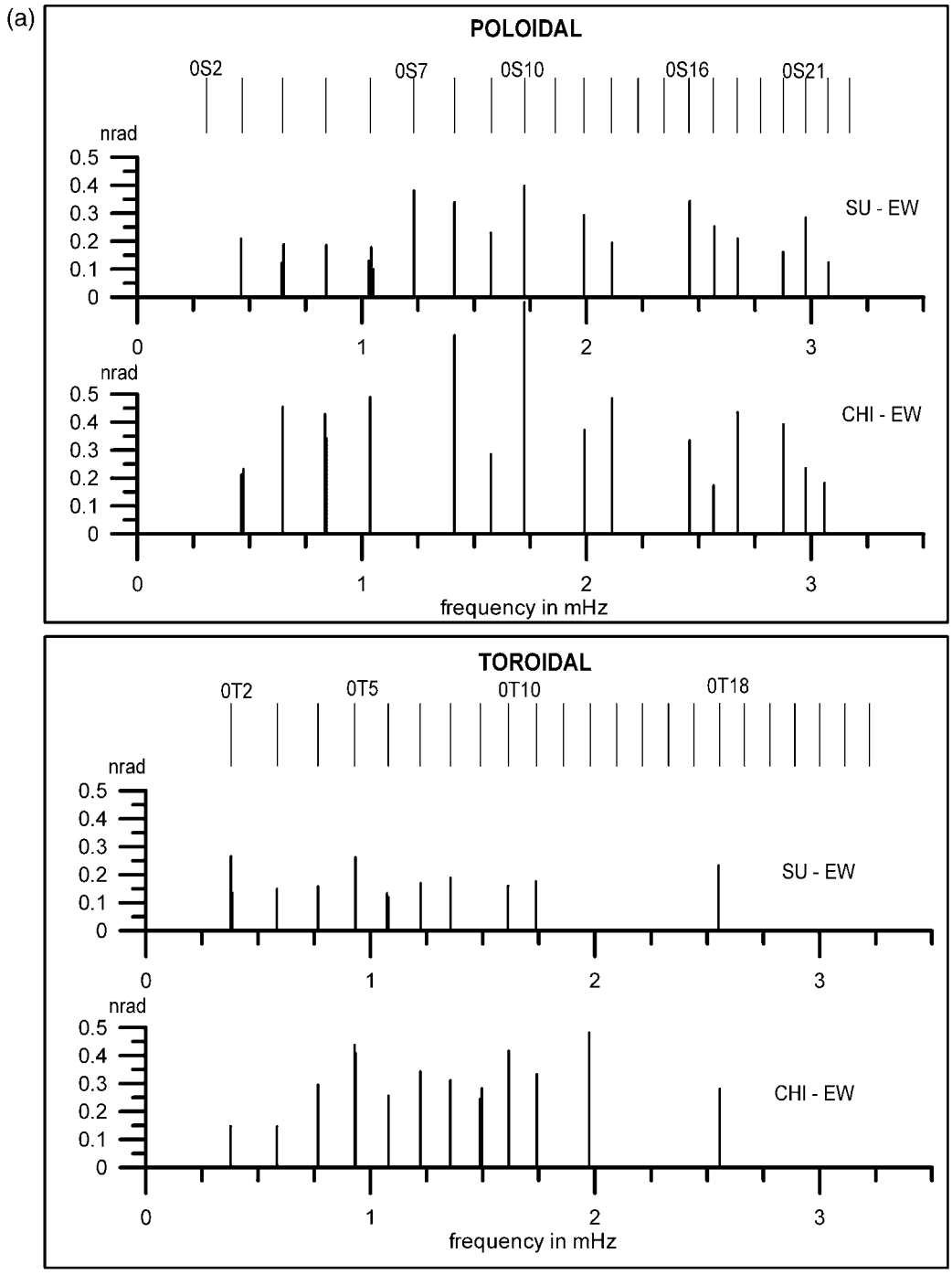


Figure 5. Amplitudes of identified fundamental and overtone ($n = 2$) modes for the Chile 1960 and Sumatra–Andaman 2004 events. (a) North–south component: poloidal ($_0S_L$) and and toroidal ($_0T_L$) modes. (b) East–west component: poloidal ($_0S_L$) and toroidal ($_0T_L$) modes. (c) North–south and east–west components: poloidal modes for overtones with overtone-index $n = 2$ ($_2S_L$). (*continued*)

amplitudes and frequencies of the free oscillation modes. For all free modes that were excited by both events, we can therefore give the amplitude ratios. Our results are the basis for the next stage of the work, which consists of the inversion of the amplitude ratios to obtain the ratio of the two moment magnitudes. We find that the amplitude ratios of the free modes excited by the Chile and Sumatra–Andaman events range between 1.5 and 3, the greater values being limited to the frequency window between 0.6 and 3 mHz. It shows that the Sumatra event has a relatively greater acti-

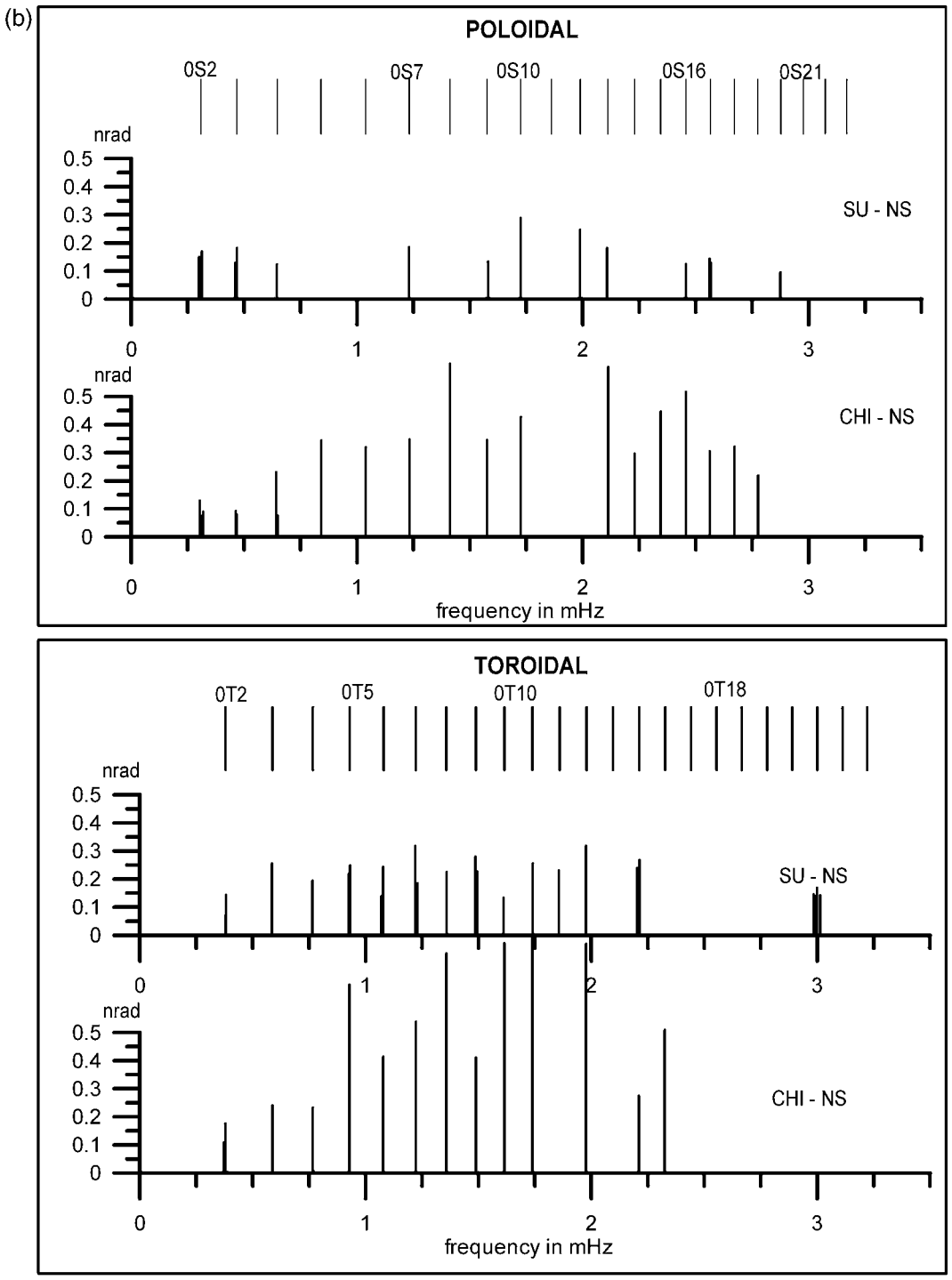


Figure 5. Continued.

vation of the lowest-order modes. At the present stage of the work, the amplitude ratios have not been corrected for possible effects of nodal planes of the free modes passing through the Trieste station and distorting the amplitude ratios. We have preferred to separate the two problems: (1) the pure data of the observed amplitudes of the modes, and (2) the correction terms implying modeling of the free modes. The latter depends on the choice of the Earth model and the focal mechanism of the events.

## Data Sources

The recordings used in this article are available to the readers by request.

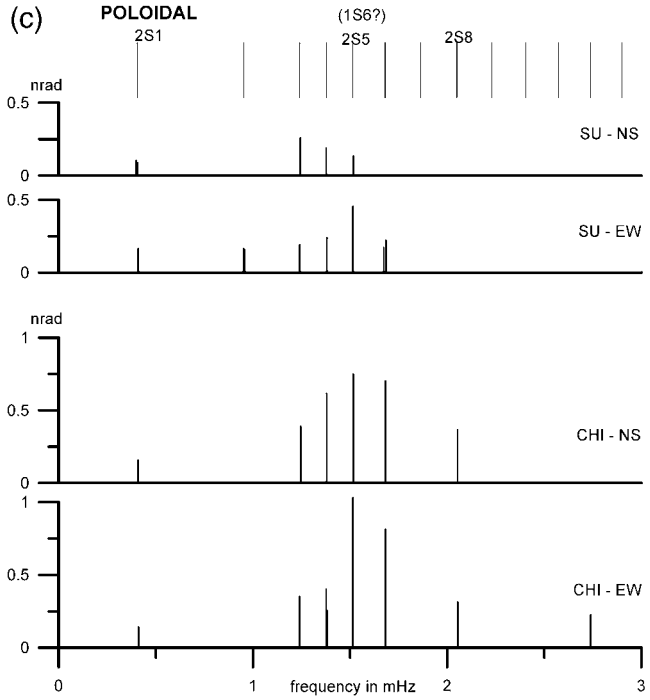


Figure 5. Continued.

The complete table of the spectral amplitudes and frequencies of the modes is attached to this article as electronic support and can be retrieved at www.units.it/~geodin/freeosc.html. The identified modes have been separated into four files that report the mode amplitudes observed with the north–south and east–west oriented pendulums, for the Chile and the Sumatra–Andaman events, respectively. The filenames are ChiEWeigen.dat, ChiNSeigen.dat, SuE Weigen.dat, SuNSeigen.dat, with obvious association of the file names to the spectrum in question. The three file columns report the observed mode frequency, the mode name, and the observed spectral amplitude.

## Acknowledgments

We thank Dr. Ildikò Nagy for help with the data preparation. Sergio Zidarich is thanked for technical maintenance of the stations. Gerhard Jentzsch (Friedrich Schiller Universität Jena) and an anonymous reviewer are thanked for their reviews. Rudolf Widmer-Schnidrig and Walter Zürn (Black Forest Observatory, Wolfach) are thanked for helpful suggestions. This work was made with the contribution of the Istituto Nazionale di Geofisica e Vulcanologia and the Italian Department for Civil Defence.

## References

Alsop, L. E., G. H. Sutton, and M. Ewing (1961). Free oscillations of the earth observed on strain and pendulum seismographs, *J. Geophys. Res.* **66,** 631–641.

Ammon, C. J., C. Ji, H.-K. Thio, D. Robinson, S. Ni, V. Hjorleifsdottir, H. Kanamori, T. Lay, S. Das, D. Helmberger, G. Ichinose, J. Polet, and D. Wald (2005). Rupture process of the 2004 Sumatra–Andaman earthquake, *Science* **308,** 1133–1139.

Angermann, D., J. Klotz, and C. Reigber (1999). Space-geodetic estimation of the Nazca–South America Euler vector, *Earth Planet. Sci. Lett.* **171,** 329–334.

Barrientos, S. E., and S. N. Ward (1990). The 1960 Chile earthquake: inversion for slip distribution from surface deformation, *Geophys. J. Int.* **103,** 589–598.

Benioff, H., F. Press, and S. Smith (1961). Excitation of the free oscillations of the earth by earthquakes, *J. Geophys. Res.* **66,** 605–619.

Bolt, B. A., and R. G. Currie (1975). Maximum entropy estimates of earth torsional eigenperiods from 1960 Trieste data, *Geophys. J. R. Astr. Soc.* **40,** 107–114.

Bolt, B. A., and A. Marussi (1962). Eigenvibrations of the earth observed at Trieste, *Geophys. J. R. Astr. Soc.* **6,** 299–311.

Bozzi Zadro, M., and A. Marussi (1967). Polarization and total energy spectra of the eigenvibrations of the earth recorded at Trieste, *Geophys. J. R. Astr. Soc.* **12,** 425–436.

Braitenberg, C. (1999). The Friuli (NE Italy) tilt/strain gauges and short term observations, *Annali di Geofisica* **42,** 1–28.

Braitenberg, C., and M. Zadro (1999). The Grotta Gigante horizontal pendulums—instrumentation and observations, *Boll. Geof. Teor. Appl.* **40,** 577–582.

Braitenberg, C., I. Nagy, G. Romeo, and Q. Taccetti (2004). The very broad-band data acquisition of the long-base tiltmeters of Grotta Gigante (Trieste, Italy), in *Progress in Geodesy and Geodynamics*, Zhu Yaozhong and Sun Heping (Editors), Hubei Science and Technology Press, Wuhan, 457–462.

Braitenberg, C., G. Romeo, Q. Taccetti, and I. Nagy (2005). The very-broad-band long-base tiltmeters of Grotta Gigante (Trieste, Italy): secular term tilting and the great Sumatra–Andaman Islands earthquake of December 26, 2004, *J. Geodynamics* **41,** 164–174.

Buchheim, W., and S. W. Smith (1961). The Earth's free oscillations observed on earth tide instruments at Tiefenort, East Germany, *J. Geophys. Res.*, **66,** 3608–3610.

Cifuentes, I. L. (1989). The 1960 Chilean earthquakes, *J. Geophys. Res.* **94,** 665–680.

Cifuentes, I. L., and P. Silver (1989). Low-frequency source characteristics of the great 1960 Chilean earthquake, *J. Geophys. Res.* **94,** 643–664.

Dahlen, F. A., and R. V. Sailor (1979). Rotational and elliptical splitting of the free oscillations of the Earth, *Geophys. J. R. Astr. Soc.* **58,** 609–623.

DeMets, C., R. G. Gordon, D. F. Argus, and S. Stein (1994). Effect of recent revisions to the geomagnetic reversal time scale on estimates of current plate motions, *Geophys. Res. Lett.* **21,** no. 20, 2191–2194.

Global Centroid Moment Tensor (CMT) Project catalog search, www.globalcmt.org/CMTsearch.html (last accessed October 2006).

Hu, Y., K. Wang, J. He, J. Klotz, and G. Khazaradze (2004). Three-dimensional viscoelastic finite element model for postseismic deformation of the great 1960 Chile earthquake, *J. Geophys. Res.* **109,** B12403, doi 10.1029/2004JB003163.

Kanamori, H. (1977). The energy release in great earthquakes, *J. Geophys. Res.* **82,** 2981–2987.

Kanamori, H., and J. Cipar (1974). Focal process of the great Chilean earthquake May 22, 1960, *Phys. Earth Planet. Interiors* **9,** 128–136.

Lay, T., H. Kanamori, C. J. Ammon, M. Nettles, S. N. Ward, F. R. C. Aster, S. L. Beck, S. L. Bilek, M. R. Brudzinski, R. Butler, H. R. DeShon, G. Ekström, K. Satake, and S. Sipkin (2005). The great Sumatra–Andaman earthquake of 26 December 2004, *Science* **308,** 1127–1133.

Lund, F. (1983). Interpretation of the precursor to the 1960 great Chilean earthquake as a seismic solitary wave, *Pageoph* **121,** 17–26.

Marussi, A. (1959). The University of Trieste station for the study of the tides of the vertical in the Grotta Gigante, in *Proc. III International Symposium on Earth Tides*, Trieste, Italy, 45–52.

Park, J., T. A. Song, J. Tromp, E. Okal, S. Stein, G. Roult, E. Clevede, G. Laske, H. Kanamori, P. Davis, J. Berger, C. Braitenberg, M. Van Camp, X. Lei, H. Sun, H. Xu, and S. Rosat (2005). Earth's free oscillations excited by the 26 December 2004 Sumatra–Andaman earthquake, *Science* **308,** 1139–1144.

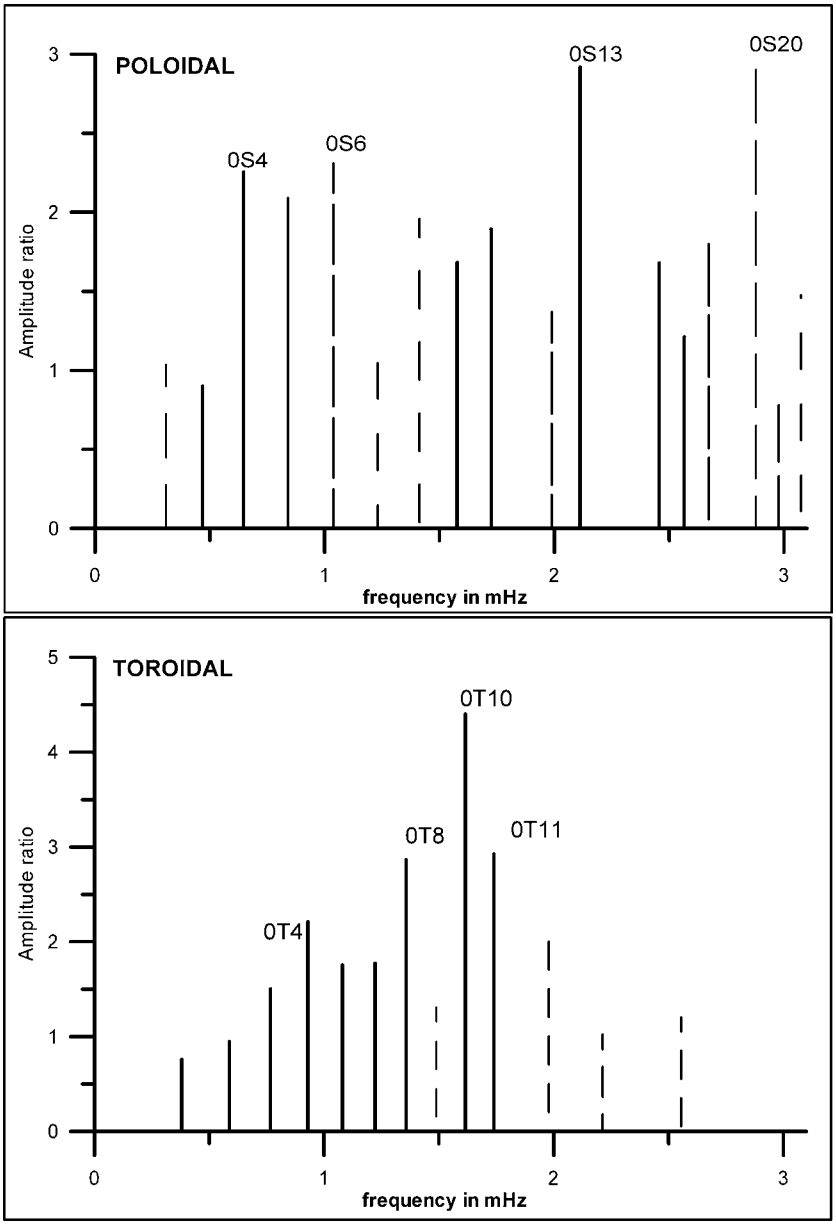


Figure 6. Ratio of the free-mode amplitudes excited by the Chile 1960 and Sumatra–Andaman 2004 events. The graph shows the results for the poloidal and toroidal modes. The frequencies at which the mode was identified on both components of both events are given with a continuous line; those at which not all components showed the mode are identified as dashed lines.

Stein, S., and E. Okal (2005). Speed and size of the Sumatra earthquake, *Nature* **434,** 581–582.

Talley, H. C., Jr., and W. K. Cloud (1962). United States Earthquakes, 1960, U.S. Coast and Geod. Surv., Washington, D.C.

Zadro, M., and C. Braitenberg (1999). Measurements and interpretations of tilt-strain gauges in seismically active areas, *Earth Sci. Rev.* **47,** 151–187.

Department of Earth Sciences
Trieste University
Via Weiss 1
34100 Trieste, Italy
maria.zadro@alice.it
berg@units.it

Manuscript received 18 January 2006.